Journal of Catalysis 398 (2021) 133–147

Contents lists available at ScienceDirect

Journal of Catalysis

journal homepage: www.elsevier.com/locate/jcat

From the grafting of NHC-based Pd(II) complexes onto TiO_2 to the *in situ* generation of Mott-Schottky heterojunctions: The boosting effect in the Suzuki-Miyaura reaction. Do the evolved Pd NPs act as reservoirs?

Jonathan De Tovar [a,b,*], Franck Rataboul [a], Laurent Djakovitch [a,*]

[a] Université de Lyon, Université Claude Bernard Lyon 1, CNRS, IRCELYON, F-69626 Villeurbanne, France
[b] Université Grenoble Alpes, CNRS, CEA, IRIG, Laboratoire de Chimie et Biologie des Métaux, 17 rue des Martyrs, Grenoble 38000, France

ARTICLE INFO

Article history:
Received 13 January 2021
Revised 23 March 2021
Accepted 12 April 2021
Available online 21 April 2021

Keywords:
Suzuki-Miyaura
N-heterocyclic carbene
Palladium complexes
Palladium nanoparticles
Heterogeneous homogeneous catalysis
Titania

ABSTRACT

The assumption that the real active species involved in the Suzuki-Miyaura reaction are homogeneous, heterogeneous or both is often proposed. However a lack of characterization of the true catalytic entities and their monitoring makes assumptions somewhat elusive. Here, with the aim of getting new insights into the formation of active species in the Suzuki-Miyaura reaction, a family of palladium(II) complexes bearing bis(NHC) ligands was synthesized for immobilization at the surface of TiO_2. The studies reveal that once the complexes are anchored onto TiO_2, the mechanism governing the catalytic reaction is different from that observed for the non-anchored complexes. All complexes evolved to Pd NPs at the surface of TiO_2 under reaction conditions and released Pd species in the liquid phase. Also, this reactivity was boosted by the *in situ* generation of Mott-Schottky heterojunctions, opening new routes towards the design of heterogenized catalysts for their further implementation in reverse-flow reactors.

1. Introduction

Palladium-based catalysts play an important role in C-C cross-coupling reactions [1]. In particular, the impact of the Suzuki-Miyaura reaction has been immense since it has resulted to be one of the most efficient methodologies for the formation of biaryl derivatives [2].

Despite the fact that many palladium-based complexes exhibiting high performances have been developed, the recovery and reuse of the catalytic system is still problematic. To tackle this issue the heterogenization of the complexes by immobilization onto a support is a possibility [3,4,5,6,7]. However, the catalytic activity of such systems is usually lower than that of the homogeneous ones. Hence, the design of more active and stable heterogenized catalysts remains a priority for C-C cross-coupling reactions.

Recently, we reported the excellent performances of novel N-heterocyclic carbene (NHC)-Pd catalysts (**C1a–c**, Scheme 1) for the Suzuki-Miyaura reaction and particularly demonstrated that the activity was strongly affected by the complex architecture [8]. In the present work we describe a comprehensive study of the heterogenization of these systems for use in Suzuki-Miyaura coupling. This corresponds to a further step towards the design of active and recyclable catalytic systems. For that we introduced a function at the ligand backbone allowing the grafting onto a support. It has been demonstrated for reported systems that the support clearly influences the catalytic performance [9,10,11,12,13]. In this view, TiO_2, exhibiting good thermal, mechanical and chemical stabilities can be regarded as a promising candidate. Therefore we particularly followed here the evolution of TiO_2-heterogenized palladium complexes of the type $PdBr_2(L \cap L)$, in which $L \cap L$ is a chelating bis(benzimidazol-2-ylidene) ligand. We aimed at identifying their catalytic performances and the nature of the active species generated from such complexes. For that we evaluated the effect of the space-length ($\cap$) of the ligand, the reaction temperature, and the recyclability of the new catalytic system.

2. Results and discussion

2.1. Synthesis and characterization of ligands and complexes

The synthetic pathway to form the hybrid materials is presented in Scheme 1. It is based on the linkage of two benzimidazole **1** moieties giving bisbenzimidazolealkanes **2a–c** [14] followed by an alkylation with diethyl (3-bromopropyl)phosphonate leading to ligands **3a-c**. These were fully characterized by ^{1}H, ^{13}C and ^{31}P NMR spectroscopies (1D and 2D spectra, see Experimental section,

* Corresponding authors.
E-mail addresses: Jonathan.DeTovarVillanueva@cea.fr (J. De Tovar), Laurent.Djakovitch@ircelyon.univ-lyon1.fr (L. Djakovitch).

https://doi.org/10.1016/j.jcat.2021.04.016
0021-9517/

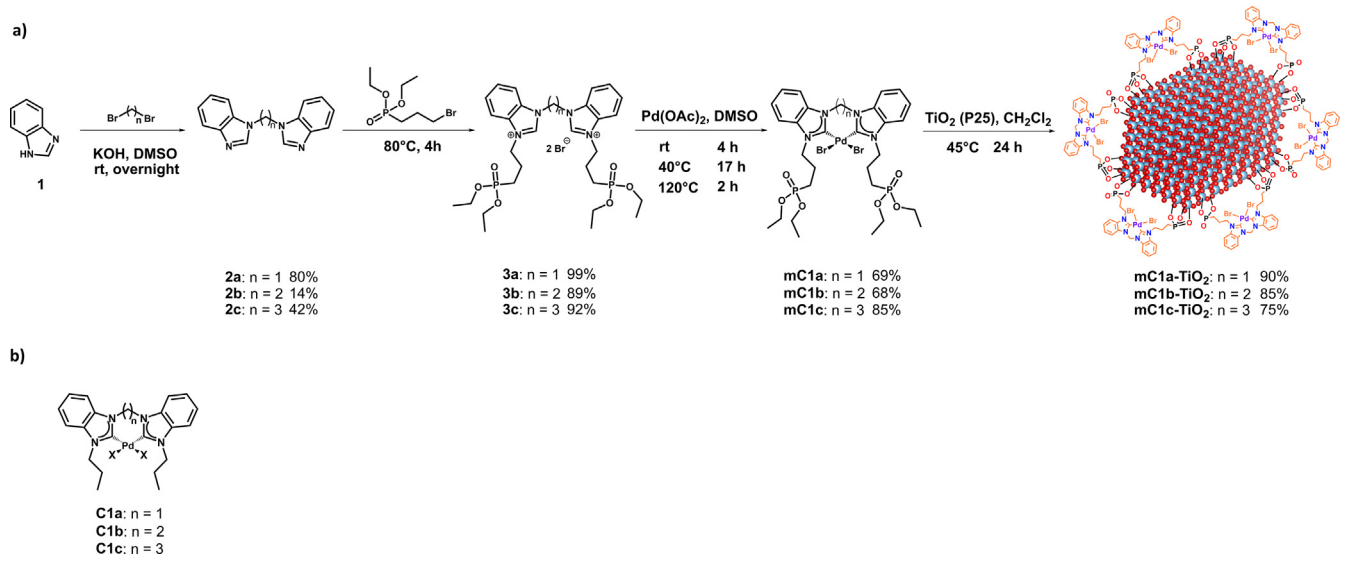

Scheme 1. (a) Synthetic pathway for **3a-c** ligands, **mC1a-c** complexes and **mC1a-c**-TiO_2 hybrid catalysts. (b) **C1a-c** complexes prepared in our previous study (reference [8]).

Figures S1–S3). Here note that ^{1}H NMR indicates a C_2 symmetry in solution for the three ligands in which not only the two alkylated benzimidazolium moieties are equivalent but also bridge protons. All ligands have also been characterized by HR-ESI-MS (Figures S4–S6) and IR spectroscopies (Figures S7–S9).

Next, coordination to $Pd(OAc)_2$ gave corresponding palladium (II) molecular complexes **mC1a-c** obtained as air- and moisture-stable solids. ^{1}H NMR spectra show that the downfield signals (~9–11 ppm) of acidic protons for the different bisbenzimidazolium salts are no longer present (Figures S10–S12), confirming the deprotonation of the benzimidazolium moiety upon formation of biscarbene complexes [15]. Additionally, all methylene protons of the bridges become diastereotopic due to ligand coordination and retention of the bend-boat conformation in these complexes [16]. The observed broadening of these resonances has been attributed to the fluxionality of the seven- or eight-membered chelate rings [17]. Interestingly, the methylene protons of propyl chains became also diastereotopic because of the H···Br interaction with bromido ligands, these methylene protons being shifted downfield (4–5 ppm). The formation of the **mC1a-c** mononuclear complexes was also supported by their high-resolution ESI mass spectra at m/z = 892.9868, 907.0019 and 921.0180 for the molecular cations $[M + Na]^+$ (**mC1a, mC1b** and **mC1c**, respectively, Figures S13–S16), fitting with their simulated spectra. Finally, the complexes have been complementary characterized by IR spectroscopy (Figures S16–S18).

2.2. Anchoring of the complexes on TiO_2

The next step consisted in grafting the **mC1a-c** Pd(II) complexes at the surface of TiO_2 (P-25, see Experimental section) to form the hybrid materials (**mC1a-c**-TiO_2) (Scheme 1).

Phosphonate anchoring groups are well known to efficiently interact with metal oxide surfaces [18,19,20]. For instance, the cleavage of P-OEt bonds on TiO_2 has already been reported in the case of diethyl phenylphosphonate [21]. Here the grafting was performed following Guerrero *et al.* [22] procedure. A TiO_2 suspension in dichloromethane containing the palladium(II) complex was stirred at 45 °C for 24 h. Then, dispersion was filtered off, washed and dried at 120 °C under vacuum. ICP-OES analyses indicated that the grafting was achieved with 68 to 82% yield (Table 1) relative to the maximum expected 0.28 wt% Pd. Note that increasing the starting amount of Pd(II) complexes did not increase the coverage. Also, the Pd/P ratios present in the hybrid materials match with their non-grafted counterparts (see Experimental section) indicating that the integrity of the complexes remained upon grafting. The anchoring through the phosphonate moiety of **mC1a-c** complexes was attested by ATR-IR spectroscopy (Fig. 1 and S19-S20). As shown in Fig. 1 the **mC1a** complex presents two absorption bands at 1222 cm^{-1} and 1014 cm^{-1} corresponding to the free P═O and P—O—C units, respectively [22]. No free P═O and P—O—C bands are visible for **mC1a**-TiO_2 while appeared a band at 1037 cm^{-1} attributed to –P—O—Ti bond [22,23].

Table 1
Pd (wt%) and grafting (%) for the **mC1a-c**-TiO_2.

Hybrid Catalyst	Pd (wt%)	Grafting (%)
mC1a-TiO_2	0.23	82
mC1b-TiO_2	0.21	75
mC1c-TiO_2	0.19	68

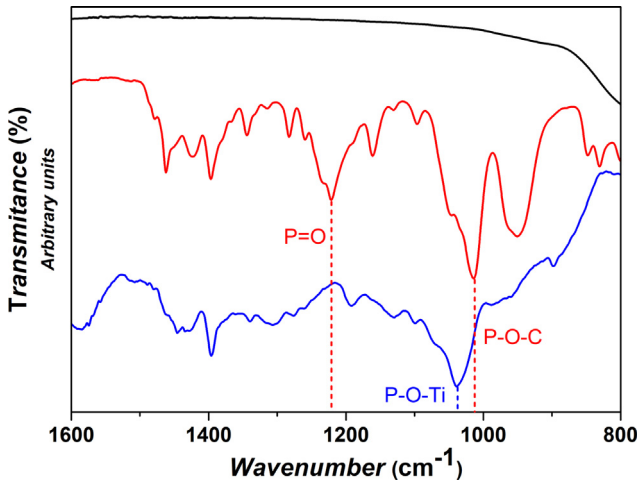

Fig. 1. Overlay of ATR-IR spectra of TiO_2 (black), **mC1a** complex (red) and **mC1a**-TiO_2 hybrid material (blue). The transmittance of each sample has been shifted along the y-axis for comparison purposes. (For interpretation of the references to colour in this figure legend, the reader is referred to the web version of this article.)

Additionally, the ^{31}P HPDEC solid-state NMR spectra of the hybrid materials (Fig. 2 and S21-S22) were similar regardless of the complex. The major resonance at 26.1 ppm is ascribed to tridentate phosphonate sites –P(OTi)$_3$. The presence of an additional resonance near 31.5 ppm points to another bonding mode, which is likely to be bidentate phosphonate –P(OTi)$_2$(OEt) sites. ^{13}C CP-MAS NMR spectra show a good match with the free **mC1a-c** complexes (Figures S23–S25).

TEM analyses of the hybrid nanomaterials revealed the presence of TiO_2 nanoobjects with a mean size of 21 nm (Figure S26). Therefore the initial size and morphology of TiO_2 were maintained after anchoring the **mC1a-c** without the decomposition of the complexes. The **mC1b**-TiO_2 and **mC1c**-TiO_2 hybrid nanomaterials were characterized accordingly, with very similar results to **mC1a**-TiO_2 (Figures S19–S22 and S24–S26).

To sum-up this section, easily obtained Pd(II) complexes bearing phosphonate moieties have been prepared and successfully grafted onto TiO_2 surface giving new hybrid nanomaterials.

2.3. Catalytic performance studies

The different prepared hybrid nanomaterials have been evaluated as catalysts for the model reaction depicted in Scheme 2, and compared with the free **C1a-c** palladium(II) molecular complexes (Scheme 1). We aimed at performing the reactions under mild conditions and short times using a low catalyst loading.

p-Bromoacetophenone and phenylboronic acid were selected as substrates in order to discriminate cross-coupling from homocouplings. Neither the homocoupling of phenylboronic acid nor that of *p*-bromoacetophenone nor dehalogenation of *p*-bromoacetophenone were observed. Thus, since the formation of *p*-acetylbiphenyl was exclusive, conversions and yields were considered as equal values. Once conditions optimized, phenylboronic acid (PhB(OH)$_2$/Pd = 1200), *p*-bromoacetophenone (substrate/Pd = 1000), and sodium methoxide (base/Pd = 1500) were employed in absolute ethanol as solvent to assure a better solubility of the former. Final conversions, turnover numbers (TONs), turnover frequencies (TOFs), initial activities (iTOFs) with induction periods are reported in Table 2 (see Experimental section for determination).

In order to compare the catalytic performance of grafted and non-grafted complexes, reactions were performed at two different temperatures of 60 °C and 25 °C using the same Pd loading (Figs. 3 and 4).

As previously observed for the free **C1a-c** complexes,[8] depletion was noted in the first 10 min (Fig. 3a) while complete conversions were achieved for all **mC1a-c**-TiO_2 (Fig. 3b). Surprisingly and

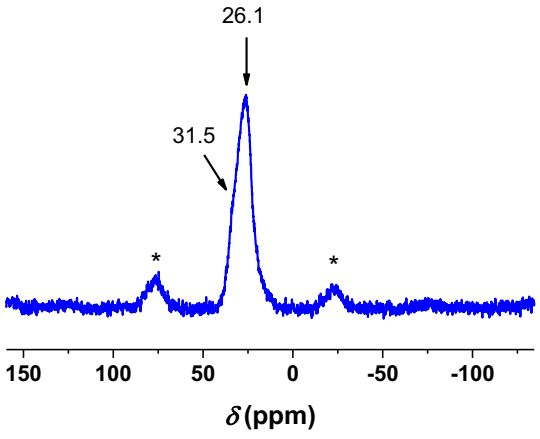

Fig. 2. ^{31}P HPDEC NMR spectrum of **mC1a**-TiO_2 hybrid material. * Spinning bands.

contrary to **C1a-c** catalysts, the performances observed for the hybrid materials led to higher iTOFs for larger bridges (Table 1). Therefore, once the complexes are grafted, the space-length (∩) affects the transformation through an opposite effect. From here, it can be inferred a different catalytic mechanism when heterogenizing the **mC1a-c** catalysts (*vide infra*, sections 2.4–2.5).

Interestingly, the new **mC1b**-TiO_2 and **mC1c**-TiO_2 materials gave moderate to good yield when decreasing the temperature to 25 °C whereas **C1a-c** complexes showed almost no activity (Fig. 4). This confirms a higher efficiency of the heterogeneous catalysts.

The formation of Pd NPs from free **C1a-c** complexes was already observed in our previous work under the same catalytic conditions [8]. Surprisingly, it appears here that even when **C1a-c** complexes are immobilized, Pd NPs were formed during the reaction as revealed by TEM images. Note that they are present not only at the surface of TiO_2 but also on the holey carbon of the TEM grid (Figures S27–S28 and Table S1). These particles exhibited a monodisperse population of spherical NPs with a narrow size-distribution. Interestingly, all NPs display a mean size lower than those evolved directly from the free **C1a-c** complexes [8]. Additionally, smaller NPs were observed after catalysis at higher temperatures. Thus, increasing the temperature greatly enhanced the complex decomposition followed by cluster formation as well as favoring the leaching of highly active Pd species from grafted Pd complexes or *in situ* formed Pd NPs.

2.4. Leaching studies

Having demonstrated the superior performance in the presence of the **mC1c**-TiO_2 catalyst for the Suzuki-Miyaura cross-coupling reaction, we addressed the leaching of the Pd-species in solution during the catalytic reaction, suspected by the formation of Pd NPs. Leaching is often observed when supported catalysts are used in such cross-coupling reactions [24,25,26] determined following several methodologies [24,27]. Among them the hot-filtration method provides reliable information. The Pd leaching was examined for the coupling reaction at 25 °C using the hot-filtration method: after 15 min of a standard catalytic run (corresponding to *ca.* 35% conversion, Fig. 5), the reaction mixture was filtered to remove **mC1c**-TiO_2 solid leaving a clear filtrate (see Experimental section). The latter was then used as reaction medium and analyzed over time. Here, the activity was completely stopped after filtration (Fig. 5). This suggests that (1) no complex degrafting occurred during this period, or (2) leached species if any were not active at 25 °C, or (3) the catalytic performance could be due to some Pd NPs formed from catalyst decomposition in the first 15 min. No Pd was found in the filtrate by ICP-OES analysis but could be present at concentration less than 0.01 ppm, that is the detection limit. With these results, to discard between the different hypotheses, we decided to increase the reaction temperature to 60 °C when using the filtrate mixture. Interestingly, at this temperature the reaction was reinitiated giving a complete conversion after 20 min (Fig. 5). This result indicates clearly that Pd species released from the immobilized palladium system or from evolved Pd NPs are present in solution. These Pd-species play a significant role in the catalyst activity at 60 °C, through homogeneous pathways. Thus, these Pd species, despite present at a very low concentration, could be the true catalytic entities and would then be redeposited on the functionalized TiO_2 or merged as Pd NPs at reaction completion.

2.5. Recycling studies

The recycling of the catalyst was examined for the coupling at 60 °C in the first 10 min. This procedure, described elsewhere,

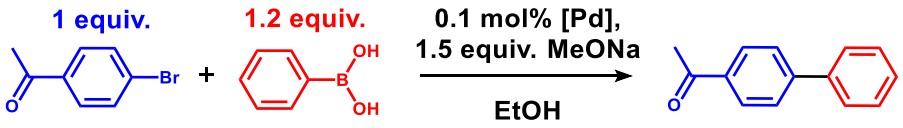

Scheme 2. Suzuki-Miyaura reaction studied in this work.

Table 2
iTOF, conversion, TON and TOF values for the Suzuki-Miyaura reaction of *p*-bromocetophenone with phenylboronic acid.

Entry	Catalyst	*p*-bromoacetophenone 60 °C iTOF ((mol product · mol Pd^{-1} · min^{-1})	Conv.	TON	TOF (h^{-1})	25 °C iTOF ((mol product · mol Pd^{-1} · min^{-1})	Conv.	TON	TOF (h^{-1})
1	**C1a**	611	100	1000	12,000	2	6	60	60
2	**C1b**	294	65	648	388	1	2	19	19
3	**C1c**	90	31	309	927	0.4	4	41	41
4	**mC1a-TiO$_2$**	169	100	1000	3000	7	10	97	97
5	**mC1b-TiO$_2$**	253	100	1000	6000	33	53	530	530
6	**mC1c-TiO$_2$**	1914	100	1000	20,000	58	83	826	826

8×10^{-4} mmol Pd, 0.8 mmol *p*-bromoacetophenone, 1 mmol phenylboronic acid and 1.2 mmol MeONa in 16 mL absolute EtOH. Conversion after 1 h reaction.

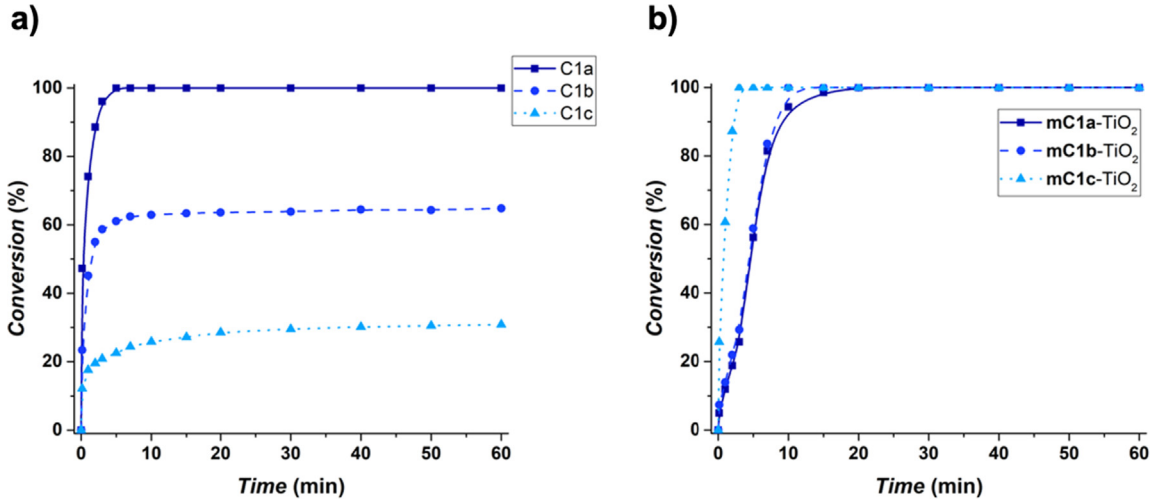

Fig. 3. Conversion versus the time for the coupling reaction of *p*-bromoacetophenone with phenylboronic acid using (a) **C1a-c** and (b) **mC1a-c-**TiO_2 catalysts at 60 °C.

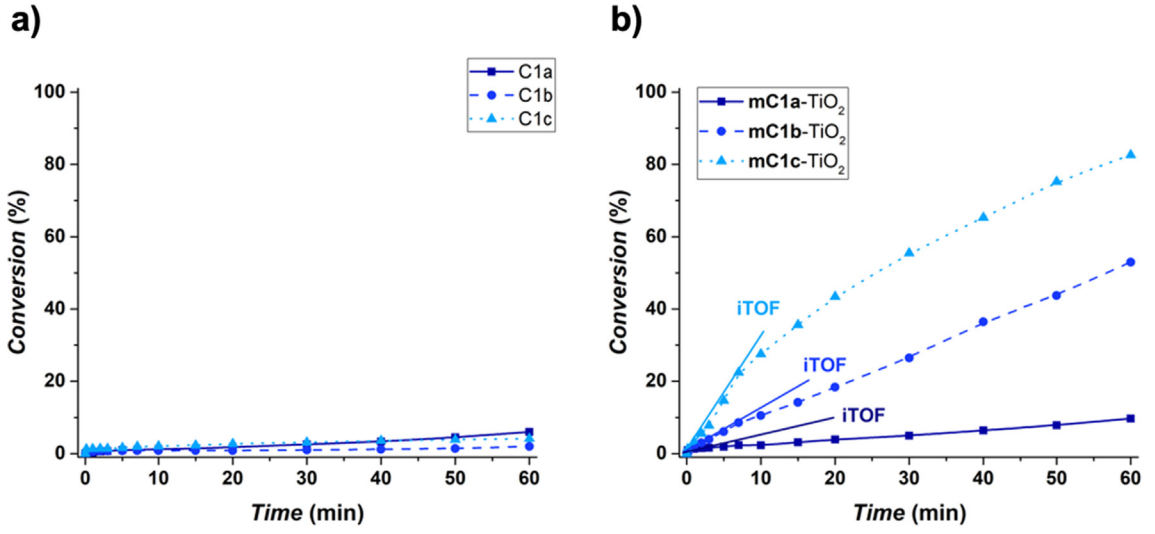

Fig. 4. Conversion versus the time for the coupling reaction of *p*-bromoacetophenone with phenylboronic acid using (a) **C1a-c** and (b) **mC1a-c-**TiO_2 catalysts at 25 °C.

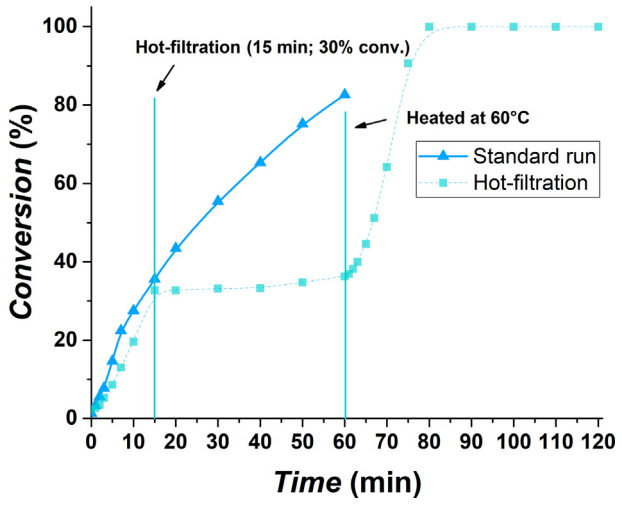

Fig. 5. Activity of **mC1c**-TiO_2 catalyst after hot-filtration at *ca.* 30% conversion versus standard catalytic run.

[28,29] was performed as follows: at the completion of a 1st run using fresh **mC1c**-TiO_2, new reagents were added to the reaction mixture and the conversion was set to 0 at the corresponding "initial time" for the next run of the catalyst (method A, see Experimental section). Fig. 6 shows that an activation occurs after the 1st run of the catalyst as indicated by determination of the initial rate $iTOF_1$ = 1914 min^{-1} for the 1st run and greater $iTOF_2$ = 5532-min^{-1} for the 2nd run (Table 3). On a one hand, only small difference was observed in terms of conversions which was completely achieved within 3 min for the 1st run whereas the 2nd run needed 10 min. To confirm the results the procedure was repeated twice. Under these conditions, comparable reaction rates $iTOF_3$ and $iTOF_4$ to that for 2nd run were observed (Table 3) indicating that no "re-activation" of the catalyst was required. On another hand, longer reaction time to achieve quantitative conversions over successive recyclings can be attributed to the visually observed change of the viscosity of the reaction mixture (increased ionic strength), preventing efficient diffusion of the substrates to the active sites.

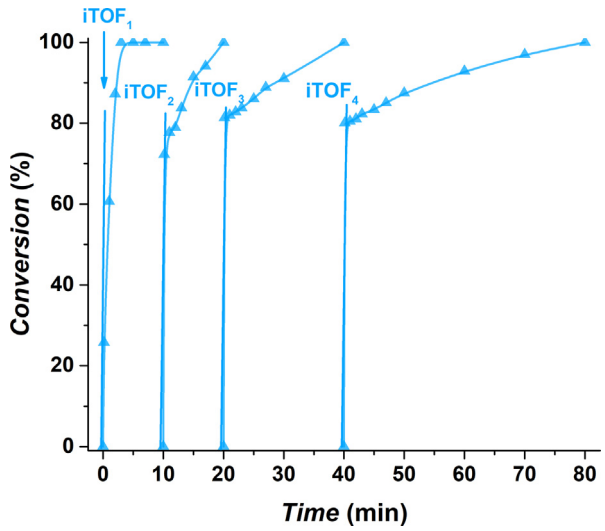

Fig. 6. Recyclability (method A) of the **mC1c**-TiO_2 catalyst for the C-C coupling of *p*-bromoacetophenone and phenylboronic acid. Reaction conditions: 8×10^{-4} mmol Pd, 0.8 mmol *p*-bromoacetophenone, 1 mmol phenylboronic acid, 1.2 mmol MeONa, 16 mL absolute EtOH, 60 °C.

In order to avoid the increased viscosity of the reaction media, the recycling tests of **mC1c**-TiO_2 were also performed by centrifugation of the reaction crude for recovery of the solid after each run (method B, see Experimental section). As shown in Fig. 7 and Table 4, lower iTOFs were obtained when reusing the separated catalyst and thus longer times were required to achieve complete conversions.

Interestingly, the filtrate collected after the 1st run (method B) was tested for possible catalytic activity. As shown in Fig. 7, it reveals, as already observed for leaching studies, the presence of species able to catalyze the reaction, at 60 °C, but rapidly deactivating as shown from the strong inflexion observed after few minutes, leading to slower overall transformation. In parallel, a complete conversion was achieved by using the filtered catalyst recovered after a 1st run (method B). Comparing to the recycling method A used previously when all species, *i.e.* dissolved Pd-species and Pd-species immobilized on TiO_2, are present at the same time, it can be inferred that the catalytic performance of **mC1c**-TiO_2 comes from both, homogeneous and heterogeneous Pd-species. This can be observed in the 2nd run when recycling the **mC1c**-TiO_2 material by method A (Table 3, 2nd run, Fig. 6). An equilibrium between the two natures of Pd-species being more probably responsible for the higher behavior observed when performing recycling by the method A. It is noteworthy to mention that the reduced efficiency of the isolated catalyst resulted from each run by method B could also be due to a deactivation upon separation from the catalytic reaction. However, as demonstrated in Figs. 6 and 7, the Pd species in the liquid phase play a pivotal role in the catalytic activity compared to the generated Pd species on TiO_2.

2.6. Fate of the catalyst and mechanism considerations

To further study the fate of **mC1c**-TiO_2 under turnover conditions, the crude reaction mixture upon recycling (method B) was analyzed by TEM, EDX, XPS, UV–Vis, solid-state ^{31}P NMR and ICP-OES.

Fig. 8 shows the evolution of the ^{31}P HPDEC NMR spectrum and indicates that the bidentate phosphonate moieties at *ca.* 31.5 ppm were partially hydrolyzed to yield a net tripodal anchoring at *ca.* 25 ppm. In parallel, TEM images reveal the presence of Pd NPs of 4.7 ± 0.6 nm both at the surface of TiO_2 and along the grid (Fig. 8 and Table 5). After the 2nd cycle, Pd NPs were only present at the surface of TiO_2 showing two families of 4.3 ± 1.0 and 17.9 ± 2.3 n m. After the 3rd cycle, a single family of Pd NPs of 4.3 ± 0.9 nm was observed. This indicates that, in fact, the evolved Pd NPs at the surface of TiO_2 act as reservoirs of active Pd species.

Additionally, the Pd and P content for the hybrid catalyst determined after each catalytic run (Table 5) indicates that the P/Pd ratio remains stable upon recycling, supporting efficient Pd redeposition on the support at reaction completion. As no P was detected in solution we exclude detachment of the ligand from the support, despite a slight increase of the Pd/P ratio in used catalyst. This explains the differentiated performance between the free **C1a-c** and **mC1a-c**-TiO_2 catalysts since the nature of the Pd NPs evolved by the latter is completely different than those evolved by the former, as already suggested by their size histograms.

To gain further insights into the effects of the state surface elemental composition, the XPS patterns for bare TiO_2, **mC1c**-TiO_2 and **mC1c**-TiO_2 (after 3rd run reused by method B) were recorded as shown in Figures S30-S33. Figure S31 shows the XPS signature of the Pd 3d doublet ($3d_{3/2}$ and $3d_{5/2}$). According to the observed binding energies, **mC1c**-TiO_2 (Figure S31, red) exhibits the Pd 3d signal at 343.38 eV (Pd $3d_{3/2}$) and 338.0 eV (Pd $3d_{5/2}$), entirely corresponding to Pd^{+2} whereas **mC1c**-TiO_2 after 3rd run reused by method B (Figure S31, blue) exhibits at 340.6 eV (Pd $3d_{3/2}$) and

Table 3
Catalyst activities, conversion, TON and TOF values for the Suzuki-Miyaura reaction of *p*-bromoacetophenone and phenylboronic acid when recycling **mC1c**-TiO_2 (method A).

Entry	iTOF (mol product · mol Pd^{-1} · min^{-1})	Conv.	TON	TOF (h^{-1})
1st run	1914	100	1000	20,000
2nd run	5532	100	1000	6000
3rd run	6235	100	1000	3000
4th run	6137	100	1000	1500

Reaction conditions: 8×10^{-4} mmol Pd, 0.8 mmol *p*-bromoacetophenone, 1 mmol phenylboronic acid and 1.2 mmol MeONa in 16 mL absolute EtOH. Conversion after 1 h reaction.

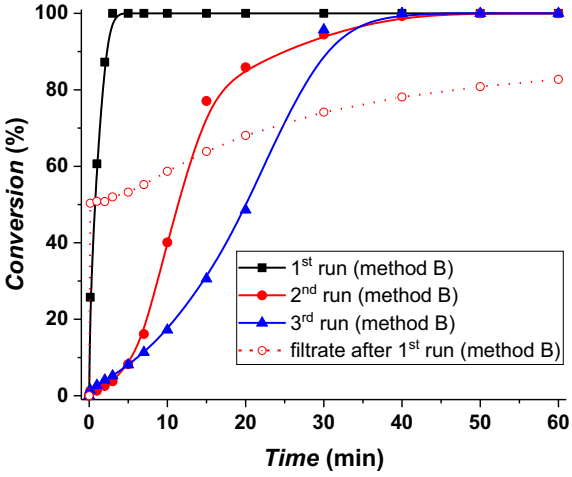

Fig. 7. Recyclability (method B) of the **mC1c**-TiO_2 catalyst for the C-C coupling of *p*-bromoacetophenone and phenylboronic acid. Reaction conditions: 8×10^{-4} mmol Pd, 0.8 mmol *p*-bromoacetophenone, 1 mmol phenylboronic acid, 1.2 mmol MeONa, 16 mL absolute EtOH, 60 °C.

335.2 eV (Pd $3d_{5/2}$), corresponding to that of bulk metallic Pd. This confirms that no decomposition of the complex occurs upon grafting and the previously observed nanoparticles are of Pd(0). Additionally, the phosphorous XPS spectra with signals are attributed to the phosphonate moieties (Figure S32) and indicate no change before and after the catalytic test. Interestingly, nitrogen XPS spectra showed that part of the benzimidazole-2-ylidene moieties were oxidized after catalysis (Figure S33).

The optical response of bare TiO_2, **mC1c**-TiO_2 and **mC1c**-TiO_2 (after 3rd run reused by method B) was recorded showing a strong absorption at less than 400 nm in all cases, which is attributed to the intrinsic absorption of TiO_2 (Figure S34). However, **mC1c**-TiO_2 (after 3rd run reused by method B) exhibited a slightly increase in absorbance in the visible and near infrared region compared to that of TiO_2.

In order to unravel the enhanced catalytic activity for **mC1a-c**-TiO_2, a new series of experiments was performed (Fig. 9 and Table 6).

First, the non-grafted **mC1c** complex (containing the phosphonate groups) was tested (Fig. 9, red, round) exhibiting a similar performance to that of **C1c** (Fig. 9, black, squares). However, two times lower iTOF was observed for this catalyst (Table 6, entry 2). This is attributed to steric hindrance due to the bulky ethyl phosphonate moieties.

Second, the role of the TiO_2 support was also studied. While no reactivity was observed with TiO_2 alone, TiO_2 in the presence of **C1c** (Fig. 9, pink, inversed triangle) gave a lower performance than that of single **C1c**. Interestingly, Pd NPs evolved under these conditions were not deposited at the surface of TiO_2 (Figure S29). Thus, the formation of Pd NPs at the surface of TiO_2 could be ascribed to their stabilization by the grafted ligands (Scheme 3). To confirm this hypothesis, the **3a** ligand (see Scheme 1) was grafted at the surface of TiO_2, yielding the **3a**-TiO_2 material (Figures S35-S36, sand Experimental section), which was introduced in the standard catalytic test in the co-presence of the **C1c** complex (see Experimental section). As shown in Fig. 10a, no depletion of the **C1c** catalyst was observed in the presence of the **3a**-TiO_2 material, achieving a complete conversion after 40 min. Additionally, the TEM image of **3a**-TiO_2 after performing the reaction (Fig. 10b) reveals the formation of Pd NPs of 1.4 ± 0.3 nm at the surface of TiO_2. This confirms the above hypothesis that ligand must be grafted onto TiO_2 to form Pd NPs at the TiO_2 surface. Also, ICP-OES analysis for the isolated hybrid catalyst provided a 0.14% Pd content. Additionally, the resulting Pd-enriched hybrid catalyst was further reused exhibiting a lower catalytic performance with *ca.* 15% conversion as shown in Figure S37. This phenomenon is attributed to a screen effect by the Pd NPs covering TiO_2.

On the other hand, when the free **mC1c** complex was tested in the presence of TiO_2 (Fig. 9, green, rhombus), a medium overall performance with an iTOF of 43 min^{-1} was observed probably due to (partial) *in situ* grafting of the complex.

Third, to elucidate the nature of the active species two separate Hg poisoning tests were performed. A large excess of Hg(0) (Hg:Pd ≈ 2000:1 mol/mol) was added to the reaction mixture at the beginning for **mC1c**-TiO_2 at 60 °C (Fig. 9, violet, right arrow). Then, the iTOF dramatically decreased to 68 min^{-1} (Table 6, entry 7). In the other experiment, when Hg(0) was added after 15 min of reaction at 25 °C, the conversion ceased completely (Fig. 11). These data also suggest that the grafted **mC1c** complex acts in fact as pre-catalyst and its evolved Pd NPs are the active species or reservoirs of them.

Fourth, since the TiO_2 P-25 support possesses semiconductor properties, we evaluated the possibility of photocatalytic assistance. For that, three different experiments were conducted. On the one hand, the **mC1c**-TiO_2 performance was studied in the dark (Fig. 9, purple, hexagon) revealing a lower iTOF (Table 6, entry 8) but a complete conversion in the first 20 min. Interestingly, when

Table 4
Catalyst activities, conversion, TON and TOF values for the Suzuki-Miyaura reaction of *p*-bromoacetophenone and phenylboronic acid when recycling **mC1c**-TiO_2 (method B).

Entry	iTOF (mol product · mol Pd^{-1} · min^{-1})	Conv.	TON	TOF (h^{-1})
1st run	1914	100	1000	20,000
2nd run	108	100	1000	1500
3rd run	102	100	1000	1500

Reaction conditions: 8×10^{-4} mmol Pd, 0.8 mmol *p*-bromoacetophenone, 1 mmol phenylboronic acid and 1.2 mmol MeONa in 16 mL absolute EtOH. Conversion after 1 h reaction.

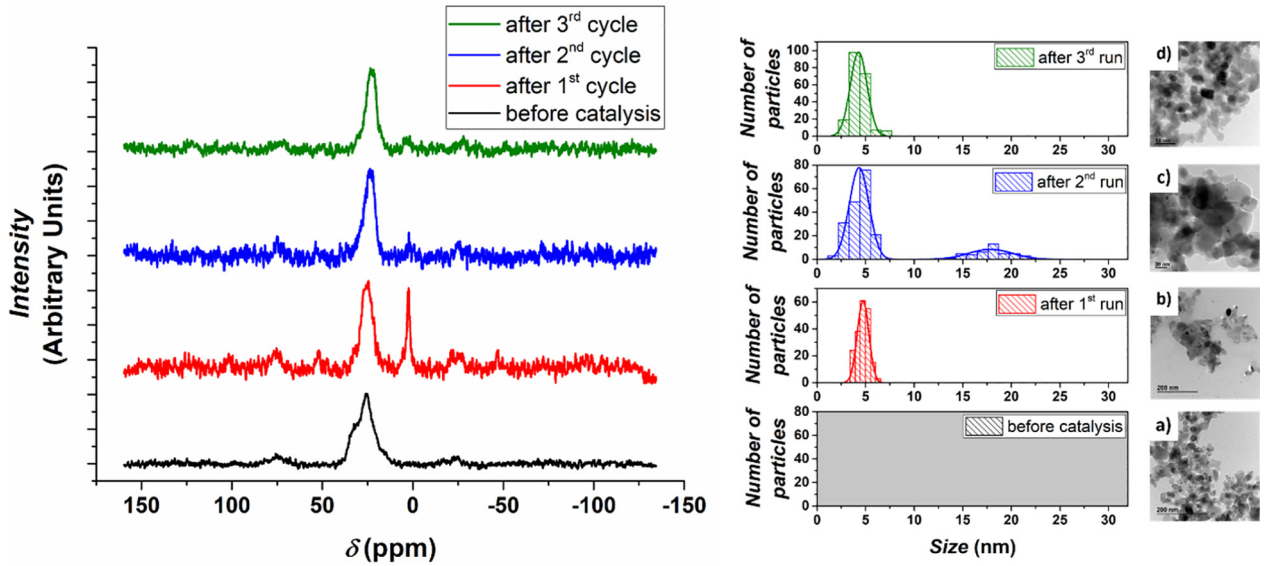

Fig. 8. Evolution of the ^{31}P HPDEC NMR for the **mC1c**-TiO_2 catalyst upon recycling and TEM images with their Pd NPs size histograms for each run (method B).

Table 5
Evolution of the mean sizes and their standard deviations for Pd nanoparticles when recycling (method B) the **mC1c**-TiO_2 catalyst using *p*-bromoacetophenone as substrate at 60 °C.

Catalyst	Mean size±standard deviation (nm)	Pd (wt%)	P (wt%)
1st run	4.7 ± 0.6	0.12	0.04
2nd run	4.3 ± 1.0; 17.9 ± 2.3	0.12	0.04
3rd run	4.3 ± 0.9	0.10	0.04

Reaction conditions: 8×10^{-4} mmol Pd, 0.8 mmol *p*-bromoacetophenone, 1 mmol phenylboronic acid and 1.2 mmol MeONa in 16 mL absolute EtOH. Data after 1 h reaction.

mC1c-TiO_2 was tested as usual but in the presence of a hole scavenger (sodium oxalate) [30] (Fig. 9, brown, stars and Table 6, entry 9), the same reactivity was observed as that in the dark. Since Ph-B$(OH)_2$ can react in basic medium to form negative Ph-B$(OH)_3^-$ species, the holes h^+ can assist in cleaving the C-B bond to produce biaryl-Pd species. Moreover, ^{11}B solid-state NMR experiments were recorded for Ph-B$(OH)_2$ (Fig. 12, black line), Ph-B$(OH)_2$ after 1 h reacting with 1.25 equivalents of MeONa in EtOH (Fig. 12, red line) and Ph-B$(OH)_2$ acid after 1 h reacting with 1.25 equivalents of MeONa in the presence of 1 equivalent of TiO_2 in EtOH (Fig. 12, blue line). The Ph-B$(OH)_2$ + OH^- ⇌ Ph-B$(OH)_3^-$ equilibrium, which presents the 55:45 ratio, was shifted to the right after the introduction of TiO_2 revealing a 36:64 ratio. Thus, these three experiments indicate that the photogenerated h^+ in TiO_2 contribute to the Ph-B$(OH)_2$-TiO_2 surface interaction accelerating the *trans*-metalation step [31]. On the other hand, when **mC1c**-TiO_2 was tested in the presence of an electron scavenger such as TEMPO (Fig. 9, olive, pentagon), a *quasi* shift relative to **mC1c**-TiO_2 was observed prompting to hypothesize that the photogenerated electrons accelerate the oxidative addition step.

Since the work function of palladium is located between the HOMO and LUMO of TiO_2 ($\Phi_{Pd} > \Phi_{TiO2}$), the formation of Pd NPs at the surface of TiO_2 results in the *in situ* generation of a rectifying metal-semiconductor contact, a Mott-Schottky heterojunction

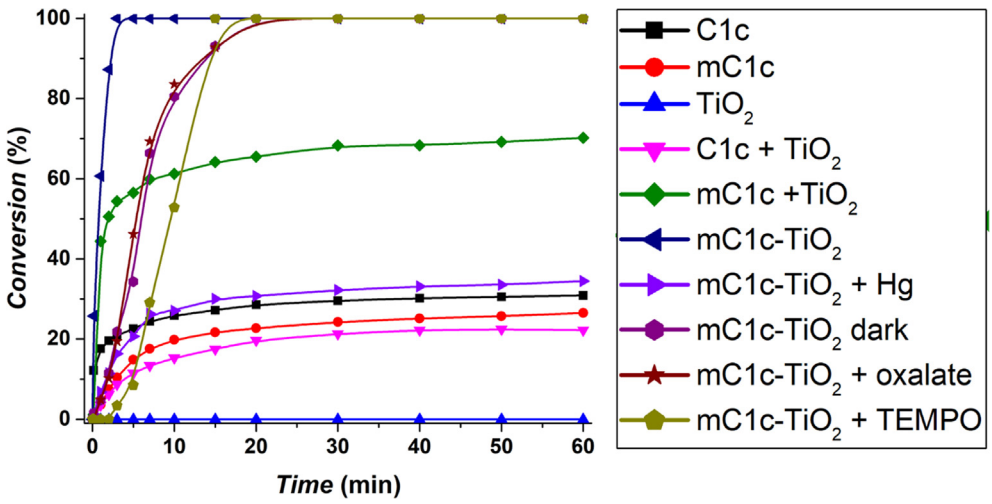

Fig. 9. Catalytic performance for the coupling of *p*-bromoacetophenone and phenylboronic acid by using (a) **C1c**, black, squares, (b) **mC1c**, red, round, (c) TiO_2, blue, triangle, (d) **C1c**+TiO_2, pink, inversed triangle, (e) **mC1c**+TiO_2, green, rhombus, (f) **mC1c**-TiO_2, navy, left arrow, (g) **mC1c**-TiO_2+Hg, violet, right arrow, (h) **mC1c**-TiO_2 in the dark, purple, hexagon, (i) **mC1c**-TiO_2+sodium oxalate, brown, stars, (j) **mC1c**-TiO_2+TEMPO, olive, pentagon. (For interpretation of the references to colour in this figure legend, the reader is referred to the web version of this article.)

Table 6
Catalyst activities, conversion, TON and TOF values for the Suzuki-Miyaura reaction of *p*-bromoacetophenone and phenylboronic acid.

Entry	Catalyst	iTOF (mol product mol Pd^{-1} min^{-1})	Induction time (min)	Conv.	TON	TOF (h^{-1})
1[8]	C1c	90	–	31	309	927
2	mC1c	43	–	27	265	530
3	TiO_2	–	–	–	–	–
4	C1c+TiO_2	41	–	22	222	444
5	mC1c+TiO_2	786	–	70	702	1404
6	mC1c-TiO_2	1914	–	100	1000	20,000
7	mC1c-TiO_2+Hg	68	–	35	345	690
8	mC1c-TiO_2 in the dark	498	–	100	1000	3000
9	mC1c-TiO_2+oxalate	421	–	100	1000	3000
10	mC1c-TiO_2+TEMPO	352	2	100	1000	4000

Reaction conditions: 8×10^{-4} mmol Pd, 0.8 mmol *p*-bromoacetophenone, 1 mmol phenylboronic acid and 1.2 mmol MeONa in 16 mL absolute EtOH. Conversion after 1 h reaction.

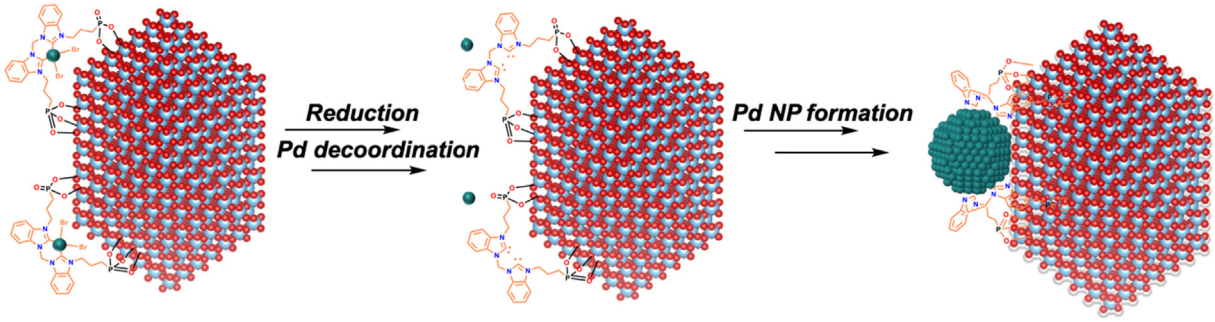

Scheme 3. Catalyst evolution of grafted Pd-bisNHC complexes at the surface of TiO_2.

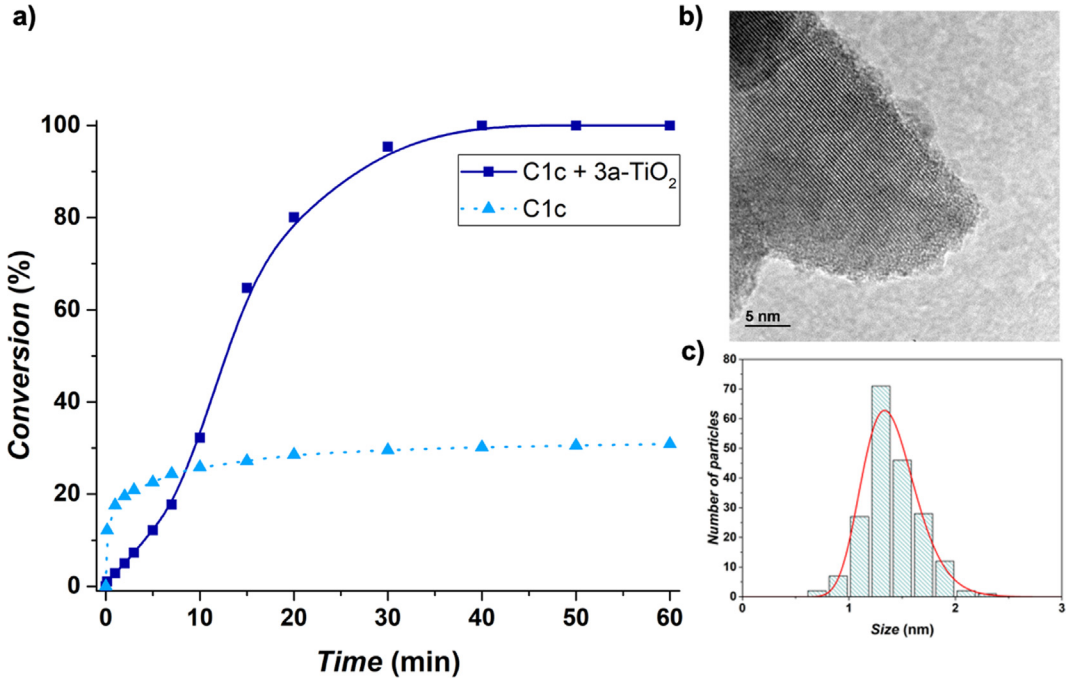

Fig. 10. (a) Comparison of the catalytic activities for the **C1c** catalyst in the absence and in the presence of the **3a**-TiO_2 material for the C-C coupling of *p*-bromoacetophenone and phenylboronic acid. Reaction conditions: 8×10^{-4} mmol Pd, 0.8 mmol *p*-bromoacetophenone, 1 mmol phenylboronic acid, 1.2 mmol MeONa, 16 mL EtOH, 60 °C. (b) TEM micrograph of the **3a**-TiO_2 material with (c) its size histogram after the catalytic reaction.

[32]. as shown in Scheme 4. Thus, a charge transfer at the interface occurs resulting in a positively charged region in TiO_2 and negatively charged Pd NPs due to the Schottky effect. The energetic e^- located at the Pd NPs and h^+ located at the TiO_2 surface can contribute to activate the *p*-bromoacetophenone and phenylboronic acid, respectively. Consequently, the Suzuki-Miyaura reaction is accelerated. However, this heterojunction can only be formed thanks to the proximity of the Pd atoms by the grafted complexes,

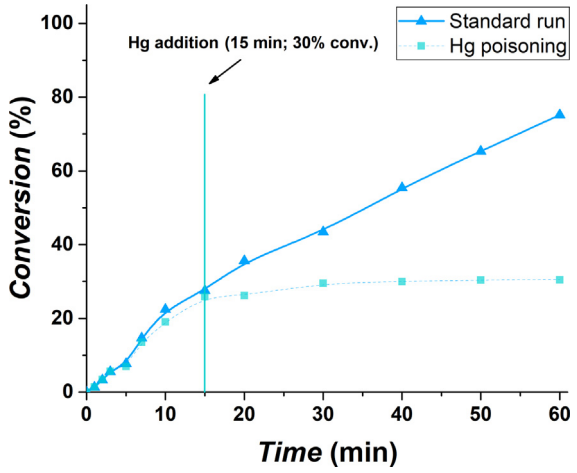

Fig. 11. Comparison of the catalytic activities for **mC1c**-TiO_2 catalyst in the absence (standard run) and after the addition of Hg (Hg poisoning) for the coupling of p-bromoacetophenone and phenylboronic acid at 25 °C.

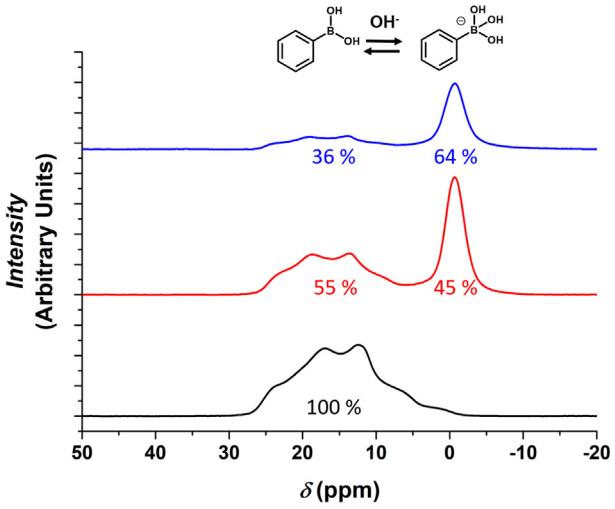

Fig. 12. ^{11}B MAS NMR spectrum for the phenylboronic acid (black line), phenylboronic acid after 1 h reaction with 1.25 equivalents of MeONa in EtOH (red line) and phenylboronic acid after 1 h reaction with 1.25 equivalents of MeONa in the presence of 1 equivalent of TiO_2 in EtOH (blue line). (For interpretation of the references to colour in this figure legend, the reader is referred to the web version of this article.)

which could be attributed to both the contribution to the Pd(II) → Pd(0) reduction by the photogenerated electrons in TiO_2 and the stabilization by the grafted ligands.

On the basis of the obtained results, we propose a mechanism (Scheme 4) in which the phenomena above mentioned take place.

2.7. Scope of the Suzuki-Miyaura reaction

Following these mechanistic studies, a reaction scope for the Suzuki-Miyaura reaction was evaluated for different aryl bromides by using **mC1c**-TiO_2 to form more functionalized products (Fig. 13). As usually observed for such coupling, aryl bromides with electron-withdrawing substituents were particularly reactive giving high yields (**4a-4 g**). Aryl bromides bearing electron-donating substituents resulted in moderate yields (**4 h-4o**). However, **4p** could not be obtained due to its reactivity under basic condition towards its enolate form, which can evolve to a quinone derivative [33]. Also, bulky aromatics provided mainly quantitative yields (**4q-4 t**). Heteroaromatics bromides were also evaluated giving in general moderate to quantitative yields for pyridyl, quinolines and isoquinolines (**4u-4y**) but 8% and 0% yield for **4v** and **4x**, respectively. However, the catalyst could not activate (benz)imidazolium bromides (**4z-4ab**), sulfur-containing heteroaromatics bromides (**4ac-4ae**), oxygen-containing heteroaromatics bromides (**4af-4ag**) and indole bromide (**4ah-4al**) but **4ak** with a moderate product yield in these conditions without substrate optimization.

3. Conclusions

We have prepared and characterized a new series of NHC-based Pd(II) complexes, which have been immobilized at the surface of TiO_2. These new hybrid materials were used as heterogeneous catalysts for the Suzuki-Miyaura reaction with the aim of providing new insights into the nature of active species in such catalysts.

First, all transformations gave quantitative yields for the coupling of *p*-bromoacetophenone and phenylboronic acid at 60 °C, and moderate to excellent yields at 25 °C. Moreover, the TOF values reached up to 20000 h^{-1} at 0.1% catalyst loading under environmentally friendly mild conditions.

Then, we have demonstrated that the heterogenized complexes not only exhibit better performances than for the corresponding homogeneous counterparts but also imply a different mechanism. Following the catalytic and recyclability studies, mercury poisoning tests, TEM and ^{31}P HPDEC NMR analyses we propose that the enhanced catalytic activities can be ascribed to the leaching of highly-active Pd species from the evolved Pd NPs at the surface of TiO_2. Interestingly for the **mC1c**-TiO_2 catalyst, we evidenced that the TiO_2 nanostructure not only serves as support but also as photoinduced boosting tool due to the *in situ* generation of Mott-Schottky heterojunctions. Thus, the photogenerated electrons in TiO_2 transferred to the Pd NPs facilitate the cleavage of the C-Br in aryl halides, while the photogenerated holes assist the cleavage of the C-B bond in the phenylboronic acid. A possible mechanism of the chemical transformation of the hybrid catalysts, the enhancing effect by TiO_2 and the leaching of Pd species is therefore proposed here pointing that the evolved Pd NPs act as reservoirs of highly-active Pd species.

Finally, after revealing the applicability of **mC1c**-TiO_2 upon recycling, a scope of substrates exhibited moderate to excellent yields for (de)activated aryl bromides as well as for sterically hindered and heteroaromatic derivatives.

4. Experimental

4.1. Materials and methods

Evonik/Degussa AEROXIDE® TiO_2 P-25 powder formed of nanoparticles of 21 nm average size was sourced from Nippon Aerosil (Yokkaichi, Japan). The rest of reagents were acquired from Sigma-Aldrich and Alfa Aesar.

All analyses were performed at IRCELYON except notified.

GC analyses were performed on a Shimadzu GC-2030 gas chromatograph equipped with a FID detector, a HP-5 column (cross-linked 5% phenylmethylsiloxane, 30 m × 0.25 mm × 0.25 μm) with helium as carrier gas. Yields were determined by GC based on the relative area of GC signals referred to an internal standard (naphthalene) calibrated to the corresponding pure compounds.

^1H NMR, ^{13}C NMR, $^{31}P\{^1H\}$ NMR, HSQC and HMBC spectra were recorded on an AVANCE III 400 Bruker spectrometer at a temperature of 25 °C. All chemical shifts were given in ppm.

^{31}P solid-state NMR spectra for hybrid materials were recorded on an AVANCE III 500WB Bruker spectrometer with the high-power decoupling (HPDEC) technique. ^{13}C solid-state NMR spectra

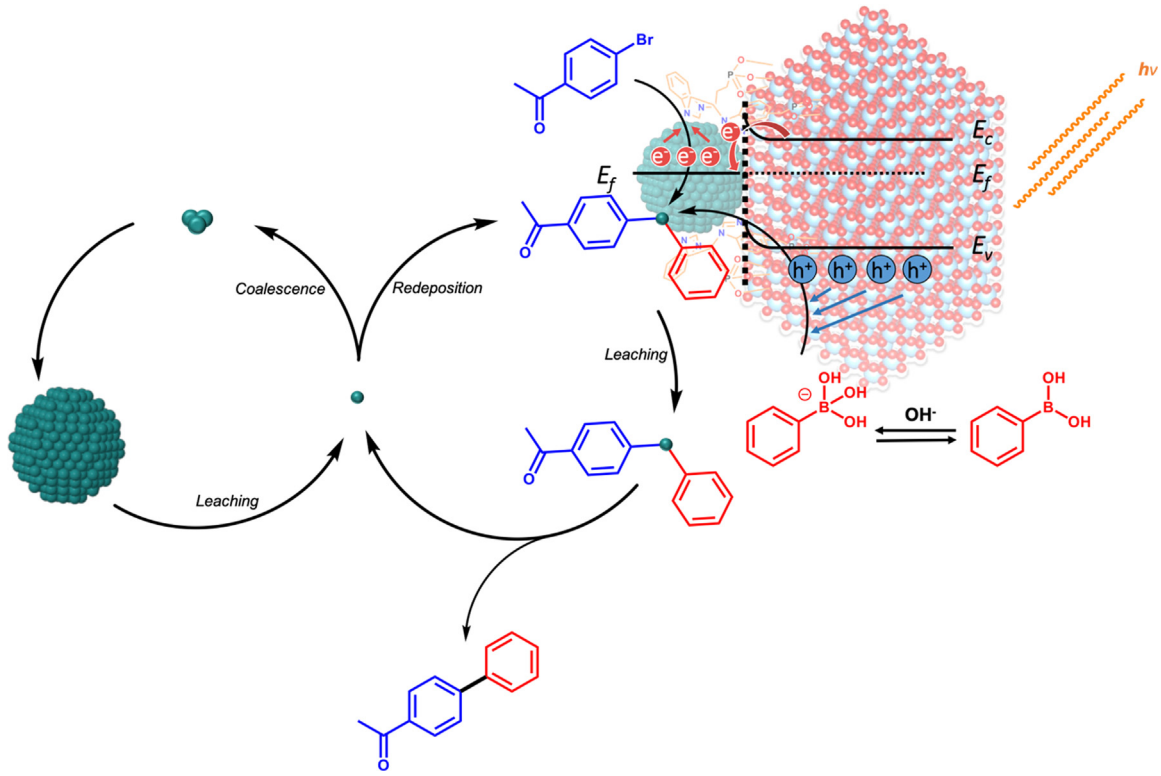

Scheme 4. Catalyst evolution and Mott-Schottky heterojunction photocatalytic contribution showing the view of the rectifying metal-semiconductor (TiO_2) contact. Legend: E_v, Valence band (HOMO); E_c, Conduction band (LUMO); E_f, work function.

for hybrid materials were recorded on an AVANCE III 500WB Bruker spectrometer with the cross-polarization magic angle spinning (CP-MAS) technique. ^{11}B solid-state NMR spectra for hybrid materials were recorded on an AVANCE III 500WB Bruker spectrometer with the magic angle spinning (MAS) technique.

The palladium content was determined on an ICP-OES ACTIVA Jobin Yvon apparatus from solutions obtained by treatment of the catalysts with sulfuric acid and aqua regia in a Teflon reactor at 400–450 °C.

Electrospray ionization Mass Spectrometry (ESI-MS) experiments were performed on a QTOF Impact II Bruker instrument equipped with an UHPLC U3000 Dionex system by the Centre Commun de Spectrométrie de Masse at the University of Lyon 1.

Transmission electron microscopy (TEM) analyses were carried out on a JEOL 2010 microscope with an instrumental magnification of 50000x to 100000x and an acceleration voltage of 200 kV. The point-to-point resolution of the microscope was 0.19 nm and the resolution between the lines was 0.14 nm. The size distributions were determined via manual analysis of enlarged images by measuring *ca.* 200 particles on a given grid to obtain a statistical size distribution and a mean diameter.

Infrared (IR) spectra were recorded with a Thermo Scientific Nicolet iS5 spectrometer in the 4000–525 cm^{-1} range in attenuated total reflectance (ATR) mode.

X-ray photoelectron spectroscopy (XPS) analyses were carried out with a Versa Probe II spectrometer (ULVAC-PHI) equipped with a monochromated Al Kα source (hν = 1486.6 eV) at CEA Grenoble. The core level peaks were recorded with constant pass energy of 23.3 eV. The XPS spectra were fitted with CasaXPS 2.3 software using Shirley background. Binding energies are referenced with respect to the adventitious carbon (C 1 s BE = 284.6 eV).

UV–Vis absorption spectra were carried out with a LAMBDA 365 UV/VIS Spectrophotometer from Pelkin Elmer (Walmar, MA, USA) in solid-state at room temperature.

4.2. Synthesis and characterization of the ligands

4.2.1. 1,1′-methylenebisbenzimidazole (2a)

A DMSO (10 mL) solution of benzimidazole (2929 mg, 24.8 mmol, 2 eq) and potassium hydroxide (5563 mg, 99.2 mmol, 8 eq) was stirred at room temperature for 1 h. Then, diiodomethane (1 mL, 12.4 mmol, 1 eq) was added at once and the reaction was stirred overnight. After the addition of water (150 mL), the product was extracted with dichloromethane (3 × 10 mL), dried over magnesium sulfate and concentrated. Diethyl ether (50 mL) was added to precipitate a white powder. Yield: 2470 mg, 80%. The spectroscopic data matched that reported in the literature.[9]

4.2.2. 1,1′-(dimethylene)bisbenzimidazole (2b)

A DMSO (10 mL) solution of benzimidazole (1000 mg, 8.46 mmol, 2 eq) and potassium hydroxide (475 mg, 8.46 mmol, 2 eq) was stirred at room temperature for 1 h. Then, dibromoethane (0.37 mL, 4.23 mmol, 1 eq) was added at once and the reaction was stirred overnight. After the addition of water (150 mL), the product was extracted with dichloromethane (3 × 10 mL), dried over magnesium sulfate and concentrated. Diethyl ether (50 mL) was added to precipitate a white powder. Yield: 154 mg, 14%. The spectroscopic data matched that reported in the literature [9].

4.2.3. 1,1′-(trimethylene)bisbenzimidazole (2c)

A DMSO (10 mL) solution of benzimidazole (1000 mg, 8.46 mmol, 2 eq) and potassium hydroxide (475 mg, 8.46 mmol, 2 eq) was stirred at room temperature for 1 h. Then, diiodopropane (0.43 mL, 4.23 mmol, 1 eq) was added at once and the reaction was stirred overnight. After the addition of water (150 mL), the product was extracted with dichloromethane (3 × 10 mL), dried over magnesium sulfate and concentrated. Diethyl ether (50 mL) was added

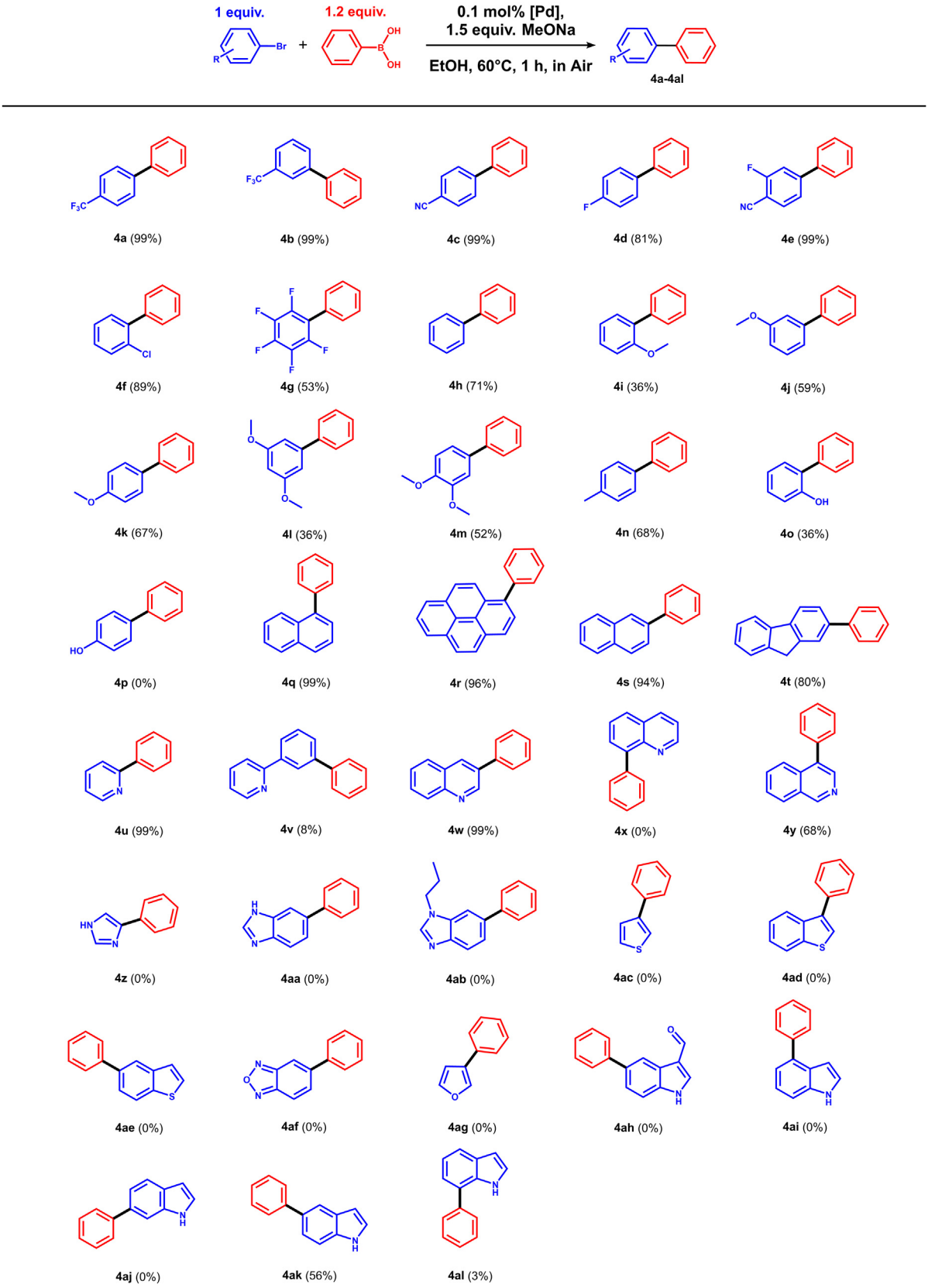

Fig. 13. Reaction scope for the coupling of aryl bromides with phenylboronic acid in the presence of the **mC1c**-TiO_2 catalyst.

to precipitate a white powder. Yield: 494 mg, 42%. The spectroscopic data matched that reported in the literature.[9]

4.2.4. 1,1′-Di(3-diethoxyphosphoryl)propyl-3,3′-methylenebisbenzimidazolium dibromide (3a)

A mixture of diethyl (3-bromopropyl)phosphonate (387 μL, 2 mmol, 2 eq) and **2a** (250 mg, 1 mmol, 1 eq) was stirred at 80 °C for 24 h. After cooling to room temperature, the crude was solved in dichloromethane (3 mL) and diethyl ether (25 mL) was added to precipitate a white off hygroscopic solid. Yield: 760 mg, 99%. ^{1}H NMR ($CDCl_3$, 25 °C): δ1.25 (t, J = 6.97 Hz, 12H, H_{12}), 1.93 (m, 4H, H_{10}), 2.38 (m, 4H, H_9), 4.03 (m, 8H, H_{11}), 4.77 (t, J = 7.46 Hz, 4H, H_8), 7.55 (t, J = 7.96 Hz, 2H, H_3), 7.65 (t, J = 7.83 Hz, 2H, H_6), 7.86 (d, J = 8.40 Hz, 2H, H_5), 8.16 (s, 2H, H_{13}), 8.74 (d, J = 8.63 Hz, 2H, H_4), 11.32 (s, 2H, H_1). ^{31}P NMR ($CDCl_3$, 25 °C): δ30.17. ^{13}C NMR ($CDCl_3$, 25 °C): δ16.5 (d, J = 5.83 Hz, C_{12}), 22.2 (d, J = 141.87 Hz, C_{10}), 22.6 (d, J = 5.00 Hz, C_9), 47.8 (d, J = 12.56 Hz, C_8), 56.5 (C_{13}), 62.2 (d, J = 6.55 Hz, C_{11}), 113.6 (C_5), 114.8 (C_4), 127.7 (C_3), 128.4 (C_6), 130.8 (C_2), 131.2 (C_7), 144.4 (C_1). IR (ATR) cm^{-1}: 2978 ν(C-H)ar, 2931 ν(C-H), 1397 (δ(C = C), δ(C = N))ar, 1215 (P = O)st, 1014 (P-O-C)st, 758 δ(C-H)oop. HR-ESI-MS (DMSO): calculated: m/z = 687.1899 ([M + Na]$^+$); found: m/z = 687.1895 ([M + Na]$^+$), 303.1362 ([M−2Br]$^{+2}$).

4.2.5. 1,1′-Di(3-diethoxyphosphoryl)propyl-3,3′-(dimethylene) bisbenzimidazolium dibromide (3b)

A mixture of diethyl (3-bromopropyl)phosphonate (147 μL, 0.76 mmol, 2 eq) and **2b** (100 mg, 0.38 mmol, 1 eq) was stirred at 80 °C for 4 h. After cooling to room temperature, the crude was filtered and washed first with dichloromethane (5 mL) and then with diethyl ether (10 mL). Yield: 244 mg, 89%. ^{1}H NMR (D_2O, 25 °C): δ1.35 (t, J = 7.18 Hz, 12H, H_{12}), 1.98 (m, 4H, H_{10}), 2.10 (m, 4H, H_9), 4.17 (m, 8H, H_{11}), 4.57 (t, J = 7.80 Hz, 4H, H_8), 5.27 (s, 4H, H_{13}), 7.36 (d, J = 8.50 Hz, 2H, H_5), 7.57 (t, J = 7.95 Hz, 2H, H_3), 7.72 (t, J = 7.70 Hz, 2H, H_6), 7.93 (d, J = 8.43 Hz, 2H, H_4), 9.44 (s, 2H, H_1). ^{31}P NMR (D_2O, 25 °C): δ33.3. ^{13}C NMR (D_2O, 25 °C): δ15.6 (d, J = 5.9 Hz, C_{12}), 21.0 (d, J = 141.6 Hz, C_{10}), 22.0 (d, J = 4.55 Hz, C_9), 46.5 (C_{13}), 47.1 (d, J = 19.4 Hz, C_8), 63.5 (d, J = 6.67 Hz, C_{11}), 111.6 (C_5), 113.7 (C_4), 127.9 (C_3 and C_6), 130.8 (C_7), 131.1 (C_2), 141.1 (C_1). IR (ATR) cm^{-1}: 2986 ν(C-H)ar, 2898 ν (C-H), 1431 (δ(C = C), δ(C = N))ar, 1222 (P = O)st, 1020 (P-O-C)st, 758 δ(C-H)oop. HR-ESI-MS (DMSO): calculated: m/z = 701.2055 ([M + Na]$^+$); found: m/z = 701.2064 ([M + Na]$^+$), 310.1442 ([M−2Br]$^{+2}$).

4.2.6. 1,1′-Di(3-diethoxyphosphoryl)propyl-3,3′-(trimethylene) bisbenzimidazolium dibromide (3c)

A mixture of diethyl (3-bromopropyl)phosphonate (348 μL, 1.8 mmol, 2 eq) and **2c** (250 mg, 0.9 mmol, 1 eq) was stirred at 80 °C for 4 h. After cooling to room temperature, the crude was solved in dichloromethane (3 mL) and diethyl ether (25 mL) was added to precipitate a white hygroscopic solid. Yield: 671 mg, 92%. ^{1}H NMR ($CDCl_3$, 25 °C): δ1.28 (t, J = 6.92 Hz, 12H, H_{12}), 1.88 (dt, J = 6.96 Hz, J = 18.57 Hz, 4H, H_{10}), 2.36 (m, 4H, H_9), 2.97 (q, J = 6.98 Hz, 2H, H_{14}), 4.06 (m, 8H, H_{11}), 4.68 (t, J = 7.48 Hz, 4H, H_8), 5.13 (t, J = 7.49 Hz, 4H, H_{13}), 7.58 (t, J = 7.99 Hz, 2H, H_5), 7.65 (t, J = 7.48 Hz, 2H, H_4), 7.78 (d, J = 8.31 Hz, 2H, H_3), 8.53 (d, J = 8.25 Hz, 2H, H_6), 10.94 (s, 2H, H_1). ^{31}P NMR ($CDCl_3$, 25 °C): δ29.8. ^{13}C NMR ($CDCl_3$, 25 °C): δ16.5 (d, J = 5.86 Hz, C_{12}), 22.2 (d, J = 135.73 Hz, C_{10}), 22.9 (d, J = 2.19 Hz, C_9), 29.6 (C_{14}), 44.5 (C_{13}), 47.2 (d, J = 11.8 Hz, C_8), 62.1 (d, J = 6.57 Hz, C_{11}), 112.7 (C_3), 115.2 (C_6), 127.5 (C_5), 127.8 (C_4), 131.0 (C_7), 131.6 (C_2), 142.0 (C_1). IR (ATR) cm^{-1}: 2978 ν(C-H)ar, 2898 ν(C-H), 1437 (δ(C = C), δ(C = N))ar, 1229 (P = O)st, 1014 (P-O-C)st, 751 δ(C-H)oop. HR-ESI-MS (DMSO): calculated: m/z = 715.2212 ([M + Na]$^+$); found: m/z = 715.2220 ([M + Na]$^+$), 317.1521 ([M−2Br]$^{+2}$).

4.3. Synthesis and characterization of the complexes

4.3.1. Dibromido-(1,1′-di(3-diethoxyphosphoryl)propyl-3,3′methylenedibenzimidazolin-2,2′-diylidene)palladium(II) (mC1a)

Palladium(II) acetate (102 mg, 0.45 mmol, 1 eq) and ligand **3a** (350 mg, 0.46 mmol, 1.01 eq) were dissolved in degassed DMSO (3 mL) in a round-bottom flask. The reddish mixture was stirred for 4 h at room temperature, 17 h at 40 °C and, finally, 2 h at 120 °C. After cooling to room temperature, dichloromethane (3 mL) was added and the crude was filtered through a plug of celite. Then, diethyl ether (50 mL) was added to the yellow solution to precipitate the product as an orange powder. Yield: 268 mg, 69%. ^{1}H NMR (DMSO d_6, 25 °C): δ1.18 (m, 12H, H_{12}), 1.86 (m, 4H, H_{10}), 2.10 (m, 4H, H_9), 3.95 (m, 8H, H_{11}), 4.60 (m, 2H, H_8), 5.01 (m, 2H, H_8), 6.79 (d, J = 13.98 Hz, 1H, H_{13}), 7.35 (d, J = 14.19 Hz, 2H, H_{13}), 7.45 (m, 4H, H_4 and H_5), 7.80 (d, J = 7.99 Hz, 2H, H_3), 8.24 (d, J = 7.92 Hz, 2H, H_6). ^{31}P{^{1}H} NMR (DMSO d_6, 25 °C): δ31.01. ^{13}C{^{1}H} NMR (DMSO d_6, 25 °C): δ16.7 (d, J = 5.23 Hz, C_{12}), 22.09 (d, J = 140.28 Hz, C_{10}), 23.1 (C_9), 48.5 (C_8), 58.0 (C_{13}), 61.5 (t, J = 7.25 Hz, C_{11}), 111.8 (C_6), 112.2 (C_3), 124.5 (C_5), 124.7 (C_4), 133.5 (C_7), 133.72 (C_2), 170.9 (C_1). IR (ATR) cm^{-1}: 3093 ν(C-H)ar, 2972 ν(C-H), 1451, 1397 (δ(C = C), δ(C = N))ar, 1222 (P = O)st, 1014 (P-O-C)st, 757 δ(C-H)oop. HR-ESI-MS (DMSO): calculated: m/z = 892.9866 ([M + Na]$^+$); found: m/z = 892.9868 ([M + Na]$^+$), 791.0794 ([M−Br]$^+$).

4.3.2. Dibromido-(1,1′-di(3-diethoxyphosphoryl)propyl-3,3′ethylenedibenzimidazolin-2,2′-diylidene)palladium(II) (mC1b)

Palladium(II) acetate (43 mg, 0.19 mmol, 1 eq) and ligand **3b** (150 mg, 0.19 mmol, 1.01 eq) were dissolved in degassed DMSO (3 mL) in a round-bottom flask. The reddish mixture was stirred for 4 h at room temperature, 17 h at 40 °C and, finally, 2 h at 120 °C. After cooling to room temperature, dichloromethane (3 mL) was added and the crude was filtered through a plug of celite. Then, diethyl ether (50 mL) was added to the yellow solution to precipitate the product as pale yellow powder. Yield: 115 mg, 68%. ^{1}H NMR (DMSO d_6, 25 °C): δ1.22 (m, 12H, H_{12}), 1.94 (m, 4H, H_{13}), 2.10 (m, 2H, H_3), 2.22 (m, 2H, H_3), 4.00 (m, 8H, H_{11}), 4.72 (m, 2H, H_{10}), 4.82 (m, 2H, H_{10}), 5.07 (m, 2H, H_2), 5.65 (m, 2H, H_2), 7.39 (m, 4H, H_5 and H_8), 7.75 (m, 4H, H_6 and H_7). ^{31}P{^{1}H} NMR (DMSO d_6, 25 °C): δ31.37. ^{13}C{^{1}H} NMR (DMSO d_6, 25 °C): δ16.3 (d, J = 5.29 Hz, C_{12}), 21.7 (d, J = 140.79 Hz, C_{13}), 22.2 (d, J = 3.86 Hz, C_3), 43.9 (C_2), 48.7 (C_{10}), 61.1 (t, J = 5.93 Hz, C_{11}), 111.3 (C_6 and C_7), 123.6 (C_5), 123.8 (C_8), 133.3 (C_4), 133.9 (C_9). IR (ATR) cm^{-1}: 2978 ν(C-H), 1464, 1404 (δ(C = C), δ(C = N))ar, 1229 (P = O)st, 1006 (P-O-C)st, 751 δ(C-H)oop. HR-ESI-MS (DMSO): calculated: m/z = 907.0023 ([M + Na]$^+$); found: m/z = 907.0019 ([M + Na]$^+$), 805.0943 ([M−Br]$^+$).

4.3.3. Dibromido-(1,1′- di(3-diethoxyphosphoryl)propyl-3,3′propylenedibenzimidazolin-2,2′-diylidene)palladium(II) (mC1c)

Palladium(II) acetate (69 mg, 0.31 mmol, 1 eq) and ligand **3c** (250 mg, 0.31 mmol, 1.01 eq) were dissolved in degassed DMSO (3 mL) in a round-bottom flask. The reddish mixture was stirred for 4 h at room temperature, 17 h at 40 °C and, finally, 2 h at 120 °C. After cooling to room temperature, dichloromethane (3 mL) was added and the crude was filtered through a plug of celite. Then, diethyl ether (50 mL) was added to the yellow solution to precipitate the product as a pale green powder. Yield: 235 mg, 85%. ^{1}H NMR (DMSO d_6, 25 °C): δ1.21 (dt, J = 12.97 Hz, J = 16.72 Hz, 12H, H_{12}), 1.87 (m, 2H, H_9 and 1H, H_{14}), 2.06 (m, 4H, H_{10}), 2.32 (m, 2H, H_9), 2.55 (m, 1H, H_{14}), 4.00 (m, 8H, H_{11}), 4.55 (td, J = 3.99 Hz, J = 10.51 Hz, 2H, H_8), 4.86 (dd, J = 5.52 Hz, J = 14.50 Hz, 2H, H_{13}), 5.05 (m, 2H, H_8), 5.26 (dd, J = 11.87 Hz, J = 14.53 Hz, 2H, H_{13}), 7.27 (dd, J = 3.09 Hz, J = 6.02 Hz, 4H, H_3 and H_6), 7.64 (m, 4H, H_4 and H_5). ^{31}P{^{1}H} NMR (DMSO d_6, 25 °C):

δ31.37. $^{13}C\{^1H\}$ NMR (DMSO d_6, 25 °C): δ16.4 (dd, J = 4.39 Hz, J = 5.72 Hz, C_{12}), 21.81 (d, J = 3.86 Hz, C_9), 21.88 (d, J = 139.59 Hz, C_{10}), 29.15 (C_{14}), 48.38 (d, J = 19.92 Hz, C_8), 48.76 (C_{13}), 61.16 (dd, J = 6.72 Hz, J = 12.21 Hz, C_{11}), 110.86 (C_5), 111.28 (C_4), 123.30 (C_6), 123.50 (C_3), 132.88 (C_7), 133.99 (C_2), 173.49 (C_1). IR (ATR) cm^{-1}: 2986 ν(C-H), 1457, 1417 (δ(C = C), δ (C = N))ar, 1229 (P = O)st, 1014 (P-O-C)st, 751 δ(C-H)oop. HR-ESI-MS (DMSO): calculated: m/z = 921.0180 ($[M + Na]^+$); found: m/z = 921.0165 ($[M + Na]^+$), 819.1093 ($[M-Br]^+$).

4.4. Synthesis and characterization of the hybrid nanomaterials

mC1a-TiO_2**:** A solution of **mC1a** (16.3 mg, 0.02 mmol, 0.002 eq) in dichloromethane (4 mL) was added to an ACE pressure tube containing TiO_2 P-25 (740 mg, 9.4 mmol, 1 eq). The reaction mixture was kept under vigorous stirring at 45 °C overnight. Then, the orange powder was filtered off and washed with dichloromethane (3 × 10 mL), methanol (3 × 10 mL) and diethyl ether (3 × 10 mL). Finally, the product was dried under vacuum at 120 °C for 6 h. Recovered: 709 mg. ^{31}P HPDEC NMR (25 °C, ppm): δ26.10, 31.55. FT-IR (ATR, cm^{-1}): 1037 (P-O-Ti) st. ICP-OES (w/w%): Pd, 0.23; Ti, 56.12; P, 0.11.

mC1b-TiO_2**:** A solution of **mC1b** (16.4 mg, 0.02 mmol, 0.002 eq) in dichloromethane (4 mL) was added to an ACE pressure tube containing TiO_2 P-25 (740 mg, 9.4 mmol, 1 eq). The reaction mixture was kept under vigorous stirring at 45 °C overnight. Then, the powder was filtered off and washed with dichloromethane (3 × 10 mL), methanol (3 × 10 mL) and diethyl ether (3 × 10 mL). Finally, the product was dried under vacuum at 120 °C for 6 h. Recovered: 693 mg. ^{31}P HPDEC NMR (25 °C, ppm): δ26.02, 32.41. FT-IR (ATR, cm^{-1}): 1052 (P-O-Ti) st. ICP-OES (w/w%): Pd, 0.21; Ti, 54.38; P, 0.11.

mC1c-TiO_2**:** A solution of **mC1c** (16.9 mg, 0.02 mmol, 0.002 eq) in dichloromethane (4 mL) was added to an ACE pressure tube containing TiO_2 P-25 (740 mg, 9.4 mmol, 1 eq). The reaction mixture was kept under vigorous stirring at 45 °C overnight. Then, the powder was filtered off and washed with dichloromethane (3 × 10 mL), methanol (3 × 10 mL) and diethyl ether (3 × 10 mL). Finally, the product was dried under vacuum at 120 °C for 6 h. Recovered: 685 mg. ^{31}P HPDEC NMR (25 °C, ppm): δ25.24, 31.81. FT-IR (ATR, cm^{-1}): 1052 (P-O-Ti) st. ICP-OES (w/w%): Pd, 0.19; Ti, 55.28; P, 0.10.

3a-TiO_2**:** A solution of **3a** (15 mg, 0.019 mmol, 0.002 eq) in dichloromethane (4 mL) was added to an ACE pressure tube containing TiO_2 P-25 (600 mg, 7.6 mmol, 1 eq). The reaction mixture was kept under vigorous stirring at 45 °C overnight. Then, the powder was filtered off and washed with dichloromethane (3 × 10 mL), methanol (3 × 10 mL) and diethyl ether (3 × 10 mL). Finally, the product was dried under vacuum at 120 °C for 6 h. Recovered: 591 mg. ^{31}P HPDEC NMR (25 °C, ppm): δ25.9, 31.1. FT-IR (ATR, cm^{-1}): 1052 (P-O-Ti) st. ICP-OES (w/w%): Ti, 56.28; P, 0.29.

4.5. Catalytic experiments

4.5.1. Catalytic studies for Suzuki-Miyaura reactions

In glass tubes of a Radleys Carousel 12 Plus Station™ fitted with a water-cooled aluminum reflux head and septa, 16 mL of an absolute EtOH solution containing *p*-halogenoacetophenone (0.05 M, 1 eq), phenylboronic acid (0.06 M, 1.2 eq) and MeONa (0.075 M, 1.5 eq) were added. The reaction mixtures were stirred and heated at 25 °C or 60 °C under nitrogen atmosphere for 30 min. Then, the palladium catalyst (8×10^{-4} mmol Pd, 5×10^{-5} M, 0.001 eq) was added. The mixture was vigorously stirred and kept at 60 °C for 1 h under nitrogen. Then, an aliquot (*ca.* 0.5 mL) of the reaction crude was taken at different reaction times and quenched in a vial filled with water/ethyl acetate mixture (2:1.5, 3.5 mL) and with naphthalene (0.09 mmol) as standard.

The organic phase was analyzed by GC and GC–MS.

All products gave analytical data in agreement with those reported in the literature: {*p*-acetylbiphenyl [92–91-1], 2-methoxybiphenyl [86–26-0], 4-methoxybiphenyl [613–37-6], 4-phenyltoluene [644–08-6], 2-chloro-1,1-biphenyl [2051–60-7], 1-phenylnaphthalene [605–02-7], 1-phenylpyrene [5101–27-9], 4-phenylisoquinoline [19571–30-3], 3-phenylquinoline [1666–96-2], 2-phenylnaphthalene [612–94-2], 2-phenyl-9*H*-fluorene [28065–98-7], 3-methoxybiphenyl [2113–56-6], 2-hydroxybiphenyl [90–43-7], 3,4-dimethoxy-1,1'-biphenyl [17423–55-1], 1,3-dimethoxy-5-phenylbenzene [64326–17-6], 4-(trifluoromethyl)-1,1'-biphenyl [398–36-7], 3-(trifluoromethyl) biphenyl [366–04-1], 4-cyanobiphenyl [2920–38-9], biphenyl [613–37-6], 3-fluoro-[1,1'-biphenyl]-4-carbonitrile [503177–15-9], 4-fluorobiphenyl [324–74-3], 2,3,4,5,6-pentafluorobiphenyl [784–14-5], 2-([1,1'-biphenyl]-3-yl)pyridine [458541–39-4], 5-phenyl-1*H*-indole [66616–72-6], 7-phenyl-1*H*-indole [1863–21-4]}. For TEM analyses, a drop of the crude mixture was deposited on the holey carbon-covered copper.

In order to obtain the iTOF values, the evolved mmol of *p*-acetylbiphenyl divided by 8×10^{-4} mmol of Pd *vs* time (in minutes) was plotted. Thus, a polynomial equation was fitted for the region 0–3 min and the first derivative was calculated. Finally, the iTOF values were obtained for × = 0 for the first derivative equation. TON values were calculated dividing the evolved mmol of *p*-acetylbiphenyl by 8×10^{-4} mmol of Pd. TOF values were calculated dividing the TON values by the required time (in hours) to achieve the maximum conversion for each catalyst.

4.5.2. Procedures for recycling

Method A. After calculating the remaining volume, the appropriate amount of a stock solution of *p*-bromoacetophenone, phenylboronic acid and MeONa in EtOH (0.2 M, 0.24 M and 0.3 M, respectively) was introduced (to reach final concentrations of 0.05 M, 0.06 M and 0.075 M, respectively) in a sealed Glass catalytic reactor of the Radleys Carousel 12 Plus Station™ fitted with a water-cooled aluminum reflux head and septa. The station was preheated at 60 °C. The reaction was conducted under vigorous stirring and followed by GC analysis until completion. Then, a new aliquot of the stock solution was added keeping the same concentration of the reagents as in the previous runs.

Method B. After determining the Pd content in the hybrid catalyst, in a two-neck 250 mL round-bottom flask fitted with a reflux condenser and septa, the appropriate amounts of *p*-bromoacetophenone, phenylboronic acid and MeONa and EtOH were introduced to reach final concentrations of 0.05 M, 0.06 M and 0.075 M, respectively. The reaction mixture was preheated at 60 °C. Then, the hybrid catalyst was added at once. The reaction was conducted under vigorous stirring and followed by GC analysis until completion. Then, after cooling to room temperature, the reaction crude was centrifuged to isolate the hybrid catalyst as a powder. Furthermore, the catalyst was washed with acetone and dried under vacuum for further analyses and reuse by using the same Pd loading.

4.5.3. Catalytic performance study for C1c in the presence of 3a-TiO_2

In a glass tube of a Radleys Carousel 12 Plus Station™ fitted with a water-cooled aluminum reflux head and septa, 70 mL of an absolute EtOH solution containing *p*-bromoacetophenone (700 mg, 3.5 mmol, 0.05 M, 1 eq), phenylboronic acid (515 mg, 4.2 mmol, 0.06 M, 1.2 eq), MeONa (285 mg, 5.3 mmol, 0.075 M, 1.5 eq) and **3a**-TiO_2 (74.8 mg, 0.001 eq ligand-to-palladium) were added. The reaction mixtures were stirred and heated at 60 °C or 25 °C under nitrogen atmosphere for 30 min. Then, the palladium

catalyst **C1c** (3.5×10^{-3} mmol Pd, 5×10^{-5} M, 0.001 eq) was added from a stock solution. The mixture was vigorously stirred and kept at 60 °C for 1 h under nitrogen. Then, an aliquot (*ca.* 0.5 mL) of the reaction crude was taken at different reaction times and quenched in a vial filled with H_2O/EtOAc mixture (2:1.5, 3.5 mL) and with naphthalene (0.09 mmol) as standard. The organic phase was analyzed by GC and GC-MS.

4.5.4. Procedure for the leaching studies by hot-filtration

In glass tubes of the Radleys Carousel 12 Plus Station™ fitted with a water-cooled aluminum reflux head and septa, 16 mL of an absolute EtOH solution containing *p*-bromoacetophenone (160 mg, 0.8 mmol, 0.05 M, 1 eq), phenylboronic acid (118 mg, 0.96 mmol, 0.06 M, 1.2 eq) and MeONa (65 mg, 1.2 mmol, 0.075 M, 1.5 eq) were added. Next, the reaction mixtures were stirred and heated at 60 °C under nitrogen atmosphere for 30 min. Then, the palladium catalyst (8×10^{-4} mmol Pd, 5×10^{-5} M, 0.001 eq) was added. The reaction was conducted under vigorous stirring for 15 min of reaction. The supernatant solution was filtered through a cannula with a microglass Whatman® filter and Celite® (in order to remove all fine particles). The reaction was monitored by GC over the total period and the results compared to a standard catalytic reaction.

4.6. TEM analyses

For the hybrid **mC1a-c**-TiO_2 materials, the as-prepared powder was dispersed in EtOH followed by deposition of some drops under the holey carbon-covered copper grid. For catalytic tests, after 1 h of catalytic reaction, a drop of the crude mixture was deposited under the holey carbon-covered copper grid for TEM analysis. **mC1x**-TiO_2 catalysts were dispersed in EtOH and a drop was deposited under the holey carbon-covered copper grids.

CRediT authorship contribution statement

Jonathan De Tovar: Conceptualization, Validation, Formal analysis, Investigation, Writing - Original Draft, Writing - Review and Editing, Visualization. **Franck Rataboul:** Writing - Review and Editing, Visualization, Supervision, Project administration. **Laurent Djakovitch:** Conceptualization, Resources, Writing - Review and Editing, Visualization, Supervision, Project administration, Funding acquisition.

Declaration of Competing Interest

The authors declare that they have no known competing financial interests or personal relationships that could have appeared to influence the work reported in this paper.

Acknowledgements

Financial support from ANR research program is gratefully acknowledged (HYPERCAT, contract N° ANR-18-CE07-0021-03). We thank Dr V. Meille and Dr C. de Bellefon (CP2M, Lyon) for fruitful discussions. We kindly acknowledge L. Burel (TEM, IRCELYON, N. Bonnet and P. Mascunan (ICP-OES, IRCELYON), Dr A. Demessence (UV-vis, IRCELYON), Dr D. Aldakov (XPS, SyMMES CEA Grenoble) and the Centre Commun de Spectrométrie de Masse (University Lyon 1) for analyses and discussions.

Appendix A. Supplementary material

Supplementary data to this article can be found online at https://doi.org/10.1016/j.jcat.2021.04.016.

References

[1] S. Kotha, K. Lahiri, D. Kashinath, Recent applications of the Suzuki-Miyaura cross-coupling reaction in organic synthesis, Tetrahedron 58 (2002) 9633–9695.
[2] A. Ganesan, New tools for parallel automated chemistry, Drug Discovery Today 6 (5) (2001) 238–241.
[3] L. Yin, J. Liebscher, Carbon-carbon coupling reactions catalyzed by heterogeneous palladium catalysts, Chem. Rev. 107 (1) (2007) 133–173.
[4] V. Polshettiwar, C. Len, A. Fihri, Silica-supported palladium: sustainable catalysts for cross-coupling reactions, Coord. Chem. Rev. 253 (2009) 2599–2626.
[5] M. Lamblin, L. Nassar-Hardy, J. Hierso, E. Fouquet, F. Felpin, Recyclable heterogeneous palladium catalysts in pure water: sustainable developments in Suzuki, Heck, Sonogashira and Tsuji-Trost reactions, Adv. Synth. Catal. 352 (2010) 33–79.
[6] S. Navalón, M. Álvaro, H. García, Polymer- and ionic liquid-containing palladium: recoverable soluble cross-coupling catalysts, ChemCatChem 5 (2013) 3460–3480.
[7] K.V.S. Ranganath, S. Onitsuka, A.K. Kumar, J. Inanaga, Recent progress of N-heterocyclic carbenes in heterogeneous catalysis, Catal Sci. Technol. 3 (2013) 2161–2181.
[8] J. De Tovar, F. Rataboul, L. Djakovitch, Insights into the Suzuki-Miyaura reaction catalyzed by novel Pd – carbene complexes. are palladium – tetracarbene entities the key active species?, ChemCatChem 12 (2020) 5797–5808.
[9] A. Wolfson, O. Levy-Ontman, Recent developments in the immobilization of palladium complexes on renewable polysaccharides for Suzuki-Miyaura cross-coupling of halobenzenes and phenylboronic acids, Catalysts 10 (2020) 136.
[10] Topics in Current Chemistry, Immobilized Catalysts, A. Kirschning (Ed.), vol. 242, Springer-Verlag, Berlin Heidelberg, 2004.
[11] F. Amoroso, S. Colussi, A. Del Zotto, J. Llorca, A. Trovarelli, Room-temperature Suzuki-Miyaura reaction catalyzed by Pd supported on rare earth oxides: influence of the point of zero charge on the catalytic activity, Catal. Lett. 143 (2013) 547–554.
[12] A. Del Zotto, D. Zuccaccia, Metallic palladium, PdO, and palladium supported on metal oxides for the Suzuki-Miyaura cross-coupling reaction: a unified view of the process of formation of the catalytically active species in solution, Catal. Sci. Technol. 7 (2017) 3934–3951.
[13] A. Del Zotto, S. Colussi, A. Trovarelli, Pd/REOs catalysts applied to the Suzuki-Miyaura coupling. a comparison of their catalytic performance and reusability, Inorganic Chim Acta 470 (2018) 275–283.
[14] P.O. Asekunowo, R.A. Haque, M.R. Razali, S. Budagumpi, Benzimidazole-based silver(I) -N-heterocyclic carbene complexes as anti-bacterials: synthesis, crystal structures and nucleic acids interaction studies, Appl. Organometal. Chem. 29 (2015) 126–137.
[15] F. Gómez-Villarraga, J. De Tovar, M. Guerrero, P. Nolis, T. Parella, P. Lecante, N. Romero, L. Escriche, R. Bofill, J. Ros, X. Sala, K. Philippot, J. García-Antón, Dissimilar catalytic behavior of molecular or colloidal palladium systems with a new NHC ligand, Dalton Trans. 46 (2017) 11768–11778.
[16] T. Scherg, S.K. Schneider, S.G. Frey, J. Schwarz, E. Herdtweck, W.A. Hermann, Bridged imidazolium salts used as precursors for chelating carbene complexes of palladium in the Mizoroki-Heck reaction, Synlett 18 (2006) 2894–2907.
[17] R. Jothibasu, H.V. Huynh, Syntheses and catalytic activities of Pd(II) dicarbene and hetero-dicarbene complexes, J. Organomet. Chem. 696 (2011) 3369–3375.
[18] R. Boissezon, J. Muller, V. Beaugeard, S. Monge, J.-J. Robin, Organophosphonates as anchoring agents onto metal oxide-based materials: synthesis and applications, RSC Adv. 4 (67) (2014) 35690, https://doi.org/10.1039/C4RA05414H.
[19] S.A. Paniagua, A.J. Giordano, O.L. Smith, S. Barlow, H. Li, N.R. Armstrong, J.E. Pemberton, J.-L. Brédas, D. Ginger, S.R. Marder, Phosphonic acids for interfacial engineering of transparent conductive oxides, Chem. Rev. 12 (2016) 7117–7158.
[20] J. De Tovar, N. Romero, S.A. Denisov, R. Bofill, C. Gimbert-Suriñach, D. Ciuculescu-Pradins, S. Drouet, A. Llobet, P. Lecante, V. Colliere, Z. Freixa, N. McClenaghan, C. Amiens, J. García-Antón, K. Philippot, X. Sala, Light-driven water oxidation using hybrid photosensitizer-decorated Co_3O_4 nanoparticles, Mater. Today Energy 9 (2018) 506–515.
[21] M.B. Mitchell, V.N. Sheinker, E.A. Mintz, Adsorption and decomposition of dimethyl methanephosphonate on metal oxides, J. Phys. Chem. B 101 (1997) 11192–11203.
[22] G. Guerrero, P.H. Mutin, A. Vioux, Anchoring of Phosphonate and Phosphinate Coupling Molecules on Titania Particles, Chem. Mater. 13 (2001) 4367–4373.
[23] A. Bachinger, S. Ivanovici, G. Kickelbick, Formation of Janus TiO_2 nanoparticles by a pickering emulsion approach applying phosphonate coupling agents, J. Nanosci. Nanotechnol. 11 (2011) 8599–8608.
[24] L. Djakovitch, K. Koehler, J.G. De Vries, Nanoparticles and Catalysis, The Role of Palladium Nanoparticles as Catalyst for Carbon – Carbon Coupling Reactions, D. Astruc (Ed.) Wiley-VCH, Weinheim, 2008, pp. 303–348.
[25] N.T.S. Phan, M. Van Der Sluys, C.W. Jones, On the nature of the active species in palladium catalyzed Mizoroki-Heck and Suzuki-Miyaura couplings - homogeneous or heterogeneous catalysis, a critical review, Adv. Synth. Catal. 348 (2006) 609–679.

[26] G. Borja, A. Monge-Marcet, R. Pleixats, T. Parella, X. Cattoën, M. Wong Chi Man, Recyclable hybrid silica-based catalysts derived from Pd-NHC complexes for Suzuki, heck and sonogashira reactions, Eur. J. Org. Chem. (2012) 3625–3635.
[27] J.M. Richardson, C.W. Jones, Strong evidence of solution-phase catalysis associated with palladium leaching from immobilized thiols during Heck and Suzuki coupling of aryl iodides, bromides, and chlorides, J. Catal. 251 (2007) 80–93.
[28] S. Chouzier, M. Gruber, L. Djakovitch, New hetero-bimetallic Pd-Cu catalysts for the one-pot indole synthesis via the Sonogashira reaction, J. Mol. Catal. A: Chem. 212 (2004) 43–52.
[29] L. Djakovitch, P. Rollet, Sonogashira cross-coupling reactions catalyzed by copper-free palladium zeolites, Adv. Synth. Catal. 346 (2004) 1782–1792.
[30] J.A. Byrne, B.R. Eggins, Photoelectrochemistry of oxalate on particulate TiO_2 electrodes, J. Electroanal. Chem. 457 (1998) 61–72.
[31] A. Eskandari, M. Jafarpour, A. Rezaeifard, M. Salimi, Supramolecular photocatalyst of palladium (II) encapsulated within dendrimer on TiO_2 nanoparticles for photo-induced Suzuki-Miyaura and Sonogashira cross-coupling reactions, Appl. Organometal. Chem. 33 (2019) e5093.
[32] M. Sakar, R.M. Prakashi, T.-O. Do, Insights into the TiO_2-based photocatalytic systems and their mechanisms, Catalysts 9 (2019) 680.
[33] R. Santhosh Reddy, R. Mahamadali Shaikh, V. Rawat, P.U. Karabal, G. Dewkar, G. Suryavanshi, A. Sudalai, A novel synthesis and characterization of titanium superoxide and its application in organic oxidative processes catal, Suv. Asia 14 (2010) 21–32.